

Joint and Streamwise Distributed MIMO Satellite Communications with Multi-Antenna Ground Users

Parisa Ramezani, *Member, IEEE* and Emil Björnson, *Fellow, IEEE*,

Abstract—We consider a low Earth orbit downlink communication, where multiple satellites jointly serve multi-antenna ground users, transmitting multiple spatial streams per user. Using a line-of-sight-dominant satellite channel model with statistical channel state information, including angular information and large-scale fading, we study two distributed transmission modes with different fronthaul requirements. First, for joint transmission, where all satellites transmit all user streams, we formulate a sum spectral efficiency (SE) maximization problem under general convex power constraints and address the intractability of the exact ergodic SE expression by adopting a tractable approximation. Exploiting the equivalence between sum SE maximization and weighted sum mean square error minimization, we derive a novel iterative transceiver design. Second, to reduce fronthaul load, we propose streamwise transmission, where each stream is sent by a single satellite, and develop an eigenmode-based stream-satellite association using participation factors and a maximum-weight bipartite matching problem solved by the Hungarian algorithm. Numerical simulations evaluate the validity of the SE approximation, demonstrate conditions under which streamwise transmission performs nearly optimally or trades SE for lower overhead, highlight the impact of stream/user loading, and show substantial performance gains over conventional benchmarks.

Index Terms—Distributed satellite communications, statistical CSI, precoding design, multi-antenna users, streamwise transmission, bipartite matching problem.

I. INTRODUCTION

The realization of ubiquitous connectivity is formally identified by the International Telecommunication Union (ITU) as a central objective for future 6G networks, with the overarching goal of closing the global digital divide [2]. Realizing this vision requires new solutions that can deliver reliable and seamless broadband access in remote and sparsely populated regions, where deploying and maintaining terrestrial infrastructure is often economically or geographically impractical. Within this framework, satellite communication systems are expected to serve a foundational role in constructing a truly global and inclusive 6G ecosystem, complementing ground deployments by extending coverage beyond the reach of conventional networks [3], [4]. In particular, low Earth orbit (LEO) satellite systems have gained substantial momentum thanks to several advantages over geostationary (GEO) and medium Earth orbit (MEO) satellites, including significantly lower latency, propagation losses, and production and launch costs [5]–[7].

Part of this paper was submitted to the 2026 IEEE International Conference on Communications (ICC) Workshops [1]. The authors are with the Department of Communication Systems, KTH Royal Institute of Technology, 100 44 Stockholm, Sweden (email: {parram,emilbjo}@kth.se). This work is funded by the SSF research center SMART-6GSAT (Sustainable Mobile Autonomous and Resilient 6G SatCom), reg.nr. CSG23-0001.

Satellite links are inherently power-limited due to the long propagation distance, so high-gain antennas and beamforming have always been essential to concentrate radiated energy. Traditionally, beamforming has often relied on fixed analog beam patterns. Recently, the application of multiple-input multiple-output (MIMO) techniques to satellite communications has attracted growing interest, as it enables more efficient use of spatial resources and can significantly improve link performance. By exploiting multiple antennas for transmit and/or receive beamforming, satellite MIMO can concentrate energy toward intended users, mitigate interference, and improve coverage. In [8], the authors study how to bring massive MIMO into LEO satellite downlink/uplink systems while adopting full frequency reuse, where inter-beam interference becomes a key bottleneck. Since acquiring accurate instantaneous channel state information (CSI) at the satellite is often impractical in LEO settings due to large propagation delay and high mobility, the paper focuses on statistical CSI (sCSI)-based transmission design and proposes low-complexity closed-form linear designs for downlink precoding and uplink combining based on long-term channel statistics. Expanding on this, [9] investigates hybrid precoding for the downlink of a massive-MIMO LEO satellite to reduce the hardware cost and energy consumption associated with fully-digital arrays. The paper formulates a hybrid precoder design that targets energy efficiency maximization and accounts for the power consumed by radio frequency chains and the phase-shifter network. The authors of [10] develop a robust hybrid precoding scheme for a massive MIMO LEO satellite serving multiple ground users under highly dynamic channels and outdated CSI. The key idea is to formulate a risk-aware design that maximizes the satellites energy efficiency while meeting per-user rate requirements. The paper proposes a deep reinforcement learning framework with a two-stage architecture, where offline training is performed at a central terrestrial server, and the trained model is periodically delivered to the satellite for online beamforming decisions based on the current network state. In [11], the uplink of a massive MIMO LEO satellite system is studied, where multiple multi-antenna users transmit simultaneously to a multi-antenna satellite. The paper establishes structural properties of the optimal transmit covariance at each user and derives an equivalent lower-dimensional formulation that reduces the design complexity without loss of optimality. Reference [12] addresses the challenge of acquiring accurate CSI in massive MIMO LEO systems where Doppler shift causes channel aging, and proposes a decision-directed semi-blind estimation approach that refines the channel estimate by reusing detected data symbols in addition to pilots.

Taking this a step further, MIMO can be realized over

a distributed aperture by treating multiple satellites as a virtual antenna array. The concept of cell-free massive MIMO, long studied in terrestrial networks [13]–[16], is now gaining traction in satellite communications for serving ground users through such distributed transmission. By coordinating transmission across multiple satellites, this approach can improve coverage robustness, increase system capacity, and provide a more uniform user experience. However, the transmission schemes must be designed differently from terrestrial systems because one can hardly achieve phase-coherent joint transmission from multiple satellite transmitters as the differences in propagation delays and phase jitter are too large. Hence, in this paper, we will develop novel non-coherent transmission modes tailored for satellite scenarios.

A. Related Work

In [17], a two-satellite cooperative downlink scenario is investigated where the LEO satellites transmit simultaneously on the same time-frequency resource to a multi-antenna ground user. The paper introduces a stochastic analysis framework that models the user’s azimuth orientation as random, and derives the distribution of the effective channel and the resulting outage behavior for a uniform circular array at the user. The authors in [18] propose a user-centric distributed massive MIMO architecture for LEO constellations, where each ground user is served by a dynamically selected cluster of nearby satellites rather than a fixed cluster or a single satellite. The paper highlights scalability and asynchronous reception as two central implementation challenges that can disrupt joint transmission. To address these, dynamic clustering procedures are introduced that designate a reference satellite access point per user to coordinate signaling within the serving cluster and incorporate phase-aware precoding to compensate for delay-induced phase shifts. Reference [19] studies a coordinated multi-satellite multibeam downlink scenario where each LEO satellite forms a set of predefined DFT-based beams and serves many single-antenna users. The goal is to minimize the total transmit power while guaranteeing signal-to-interference-plus-noise ratio (SINR) targets, by jointly deciding which satellite each user should associate with and which small cluster of beams should be activated for that user, together with the corresponding beam-wise linear precoding weights. [20] investigates how multiple LEO satellites can cooperatively boost the received signal strength at a standard smartphone with a very limited link budget by performing distributed transmit beamforming. The paper builds an electromagnetic-wave-based model that highlights how a satellite distributed array differs from conventional phased arrays and uses this to analyze how the achievable combining gain depends on the relative satellite geometry. In [21], a dual-function LEO constellation framework is proposed that performs multi-user downlink communication and target location sensing simultaneously using the same spectrum and hardware. A central satellite cooperates with several neighboring satellites via high-capacity inter-satellite links, so that multiple satellites can jointly deliver communication signals to ground users, while also collecting target-reflected signals for sensing and fusing them at the

central satellite. The paper formulates a joint optimization that balances sensing accuracy against communication-related constraints under per-satellite power limits. A distributed multi-satellite cooperative downlink beamforming architecture for an orthogonal frequency division multiplexing (OFDM)-based LEO network is presented in [22], where satellites are connected through inter-satellite links and the transmitter relies on sCSI to design hybrid beamforming. The paper proposes a practical analog beamformer and user scheduling method, and then designs digital beamformers by maximizing a tractable lower bound on the ergodic sum rate.

These studies highlight the promising potential of joint transmission from multiple satellites to ground users, demonstrating that cooperation can strengthen weak links and improve performance through joint beamforming and interference management. However, they focus on single-antenna ground users, which inherently restricts the number of spatial degrees of freedom available at the receiver and therefore limits spatial multiplexing and stream-level processing. As state-of-the-art terrestrial and satellite receivers are typically equipped with multiple antennas, it is important to study satellite communication systems with multi-antenna ground users and exploit the additional spatial degrees of freedom to support multi-stream transmission and spatial interference cancellation. Furthermore, many of the prior works (e.g., [18], [20]–[22]) rely on coherent joint transmission from multiple satellites which may be difficult to realize in practice, since LEO satellites are widely separated and the resulting differences in propagation delays and phase jitter make tight inter-satellite synchronization challenging. Aiming to fill these gaps, in this paper, we study distributed multi-satellite MIMO with multi-antenna ground users and propose two transmission schemes with different levels of fronthaul overhead and without requiring inter-satellite phase synchronization.

B. Contributions

This paper investigates a distributed downlink satellite communication system, where multiple satellites serve multi-antenna ground users by transmitting multiple spatial data streams to each user. We consider two transmission modes: joint non-coherent transmission, where all satellites cooperatively transmit all streams to each user, and streamwise transmission, where each stream is assigned to a single satellite to reduce the fronthaul load. The contributions of this paper can be summarized as follows:

- We consider a distributed multi-satellite downlink scenario with satellites serving multi-antenna ground users by transmitting multiple spatial data streams to each user. We formulate the joint precoder design as a sum spectral efficiency (SE) maximization problem under general convex power constraints. Since the exact SE involves an expectation over fading and is analytically intractable, we adopt an approximate SE expression and reformulate the optimization problem. This reformulation yields an sCSI-based objective that is independent of the instantaneous channel phase, thereby enabling precoder design without requiring inter-satellite phase synchronization. Building on the classical equivalence between sum

SE maximization and weighted sum mean square error (MSE) minimization [23], we then derive an iterative block coordinate procedure that alternates between updating the receive combiners, MSE weights, and transmit precoders, while handling the power constraints through the associated Lagrange multipliers, which are updated using the ellipsoid method.

- To alleviate the message sharing bottleneck between the satellites and ground users, we propose a streamwise mode in which each data stream is transmitted by only one satellite. This substantially reduces the required data exchange. We then formulate a satellite-to-stream association problem to select, for each user, a subset of satellites and assign one distinct satellite to each eigenmode/stream based on their contribution to that mode. We solve the resultant maximum-weight bipartite matching problem via the Hungarian algorithm.
- Through extensive numerical simulations, we identify the regimes in which streamwise transmission is essentially lossless compared to joint transmission. Our evaluations show that when the satellite-user links are orthogonal at the user, so that each channel eigenmode is dominated by a single satellite, distributing a stream across multiple satellites brings little additional gain. In contrast, for non-orthogonal channels, joint transmission can better exploit multi-satellite interference shaping and streamwise transmission leads to a clear performance-overhead trade-off. We also observe that the number of streams and the number of simultaneously served users must be selected carefully, since aggressive spatial multiplexing under limited user-side interference suppression can diminish the gains of joint transmission. We further corroborate the proposed precoding design and stream-satellite association strategy by benchmarking them against some well-known baselines.

This work is an extended and refined version of [1]. Compared to the conference paper, which focuses on joint multi-satellite transmission and considers per-satellite and per-antenna power constraints, this paper develops a unified precoding framework under general convex power constraints, so that a wide range of practically relevant constraints can be accommodated. A key additional contribution is the proposed streamwise mode, together with an eigenmode-based stream-satellite pairing algorithm, that reduces fronthaul load while still taking advantage of multi-satellite multi-stream transmission. Overall, we broaden the problem formulation and analysis, introduce new algorithms, and expand the numerical evaluations to provide deeper insights into the performance-overhead trade-offs of distributed multi-satellite transmission with multi-antenna ground users receiving multiple spatial streams.

C. Organization

The rest of this paper is structured as follows. Section II presents the system model, formulates the sum SE maximization problem, and introduces an SE approximation that makes the problem tractable. Section III details the proposed

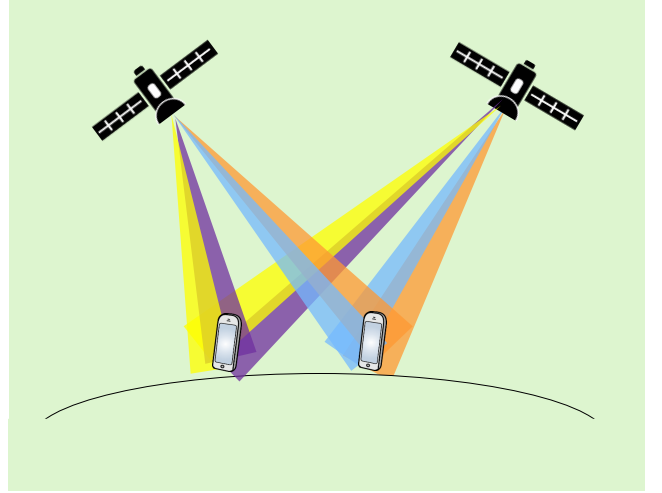


Fig. 1: Distributed multi-satellite MIMO downlink with multi-stream transmission to multi-antenna users.

precoding design for non-coherent joint transmission where all satellites transmit multiple streams to all the ground users. In Section IV, we propose a lower-overhead distributed transmission scheme where each user stream is served by a single satellite, and develop a stream-satellite association strategy. Section V provides supporting numerical simulations, and Section VI concludes the paper.

D. Notations

Scalars are denoted by italic letters, while vectors and matrices are denoted by bold-face lower-case and upper-case letters, respectively. $(\cdot)^T$ and $(\cdot)^H$ indicate the transpose and conjugate transpose, respectively, and $\Re(\cdot)$ denotes the operation of taking the real part. For the vector \mathbf{x} , $\|\mathbf{x}\|$ is its Euclidean norm and $\mathbf{x} \succ \mathbf{0}$ means that all entries of \mathbf{x} are strictly positive. For the matrix \mathbf{X} , $\|\mathbf{X}\|_F$ represents its Frobenius norm and $\mathbf{X} \succeq \mathbf{0}$ implies that \mathbf{X} is positive semidefinite. $|\mathbf{X}|$ and $\text{Tr}(\mathbf{X})$ respectively return the determinant and trace of matrix \mathbf{X} . \mathbb{C} denotes the set of complex numbers. $\mathcal{CN}(0, \omega)$ represents a circularly symmetric complex Gaussian distribution with mean 0 and variance ω and $\mathcal{CN}(\mathbf{0}, \mathbf{\Omega})$ denotes its multivariate counterpart with mean vector $\mathbf{0}$ and covariance matrix $\mathbf{\Omega}$. The operator \odot is the elementwise product, and $\mathbf{X}(i, i)$ indicates the i -th diagonal entry of \mathbf{X} . $[x]_+$ denotes clipping at zero, i.e., $[x]_+ = \max\{0, x\}$.

II. SYSTEM MODEL

As shown in Fig. 1, a downlink multi-user distributed satellite communication system is considered where a constellation of L LEO satellites (SATs), each equipped with N antennas, serve K user equipments (UEs), each having M antennas. Since the UEs have multiple antennas, multiple spatially multiplexed data streams can be sent to each UE, if the joint channel from the SATs supports it. Let $\mathbf{x}_k \sim \mathcal{CN}(\mathbf{0}, \mathbf{I}_S) \in \mathbb{C}^S$ denote the vector of $S \leq M$ data streams for UE k . The signals for different UEs are independent from each other and from

the receiver noises. With joint transmission, the received signal at UE k is

$$\mathbf{y}_k = \sum_{l=1}^L \mathbf{H}_{l,k} \mathbf{W}_{l,k} \mathbf{x}_k + \sum_{i=1, i \neq k}^K \sum_{l=1}^L \mathbf{H}_{l,k} \mathbf{W}_{l,i} \mathbf{x}_i + \mathbf{n}_k, \quad (1)$$

where $\mathbf{H}_{l,k} \in \mathbb{C}^{M \times N}$ is the channel between SAT l and UE k , $\mathbf{W}_{l,k} \in \mathbb{C}^{N \times S}$ is the precoding matrix used by SAT l for UE k 's data, and $\mathbf{n}_k \sim \mathcal{CN}(0, \sigma^2 \mathbf{I}_M)$ is the noise vector at UE k .

A. Channel Model

We consider the typical scenario in satellite communications: far-field line-of-sight (LoS) channels between the SATs and UEs. We further assume that the antenna panels at the SATs and UEs are in the form of uniform linear arrays (ULAs). Under these assumptions, the channel $\mathbf{H}_{l,k}$ can be modeled as

$$\mathbf{H}_{l,k} = \gamma_{l,k} \mathbf{b}_k(\theta_{l,k}) \mathbf{a}_l^T(\varphi_{l,k}), \quad (2)$$

where $\gamma_{l,k}$ is the complex channel gain between SAT l and UE k , $\mathbf{b}_k(\cdot)$ and $\mathbf{a}_l(\cdot)$ are respectively the array response vectors at UE k and SAT l , and $\theta_{l,k}$ and $\varphi_{l,k}$ are the respective angle-of-arrival (AoA) and angle-of-departure (AoD). The SATs typically follow precise deterministic orbital trajectories and the UEs' locations can be reliably tracked via GPS. Thus, it is reasonable to assume that the AoA and AoD information is available at the SATs and UEs [8], [9], [11], [22], [24]. However, the channel gain $\gamma_{l,k}$ varies rapidly; thus, only its statistical information is usually available at the transmitter. We model $\gamma_{l,k}$ as Rician fading with a time-varying random LoS phase and variance $\beta_{l,k}$, which accounts for rapid phase fluctuations and scattering around the UE. Specifically,

$$\gamma_{l,k} = \sqrt{\beta_{l,k}} \left(\sqrt{\frac{\kappa_{l,k}}{\kappa_{l,k} + 1}} e^{j\psi_{l,k}} + \sqrt{\frac{1}{\kappa_{l,k} + 1}} z_{l,k} \right), \quad (3)$$

where $\psi_{l,k} \sim \text{Uniform}[0, 2\pi)$, $z_{l,k} \sim \mathcal{CN}(0, 1)$, $\psi_{l,k}$ and $z_{l,k}$ are independent for all l, k , and $\beta_{l,k}$ is known a priori.

B. Sum SE Maximization Problem Formulation

The realization of $\gamma_{l,k}$ varies rapidly over time and frequency, making it suitable to measure performance in terms of the ergodic achievable SE, where the channel code spans over many random realizations. Based on the received signal expression in (1), the ergodic achievable SE at UE k is given by (4), shown at the top of the next page, where the expectation is over different channel realizations. The objective in this paper is to maximize the sum SE of all UEs by optimizing the precoding matrices at each SAT, subject to a number of convex power constraints.¹ The problem of interest is thus

¹Sum SE maximization is normally considered to provide unfair service provisioning, but the situation is different in LEO satellite communications. In these scenarios, the prospective UEs are outdoors and the SATs pass above them at high velocity, leading to very similar channel conditions on the average. Hence, every UE will get a roughly equal share of the average sum SE, and by maximizing that metric, we will provide both maximum network capacity and a high degree of fairness.

formulated as

$$\begin{aligned} & \underset{\{\mathbf{W}_{l,k}\}_{\forall l,k}}{\text{maximize}} \sum_{k=1}^K R_k, \\ & \text{subject to} \sum_{k=1}^K \text{Tr}(\mathbf{W}_{l,k}^H \mathbf{A}_{l,x} \mathbf{W}_{l,k}) \leq \rho_{l,x}, \forall l, x = 1, \dots, X_l, \end{aligned} \quad (5a)$$

$$(5b)$$

where $\mathbf{A}_{l,x} \succeq \mathbf{0}$ is a given weighting matrix that defines the x -th convex power constraint for SAT l and limits the power in a particular signal subspace of SAT l , and $\rho_{l,x}$ is the corresponding power cap for that subspace. The power constraints in (5b) represent a general model that includes many standard power constraints used in the literature. For example, the per-SAT total power constraint is obtained by setting only one constraint for each SAT ($X_l = 1 \forall l$) with $\mathbf{A}_{l,1} = \mathbf{I}_N$. Also, per-antenna power constraints are obtained by having $X_l = N \forall l$, and choosing $\mathbf{A}_{l,n} = \mathbf{E}_n$ where \mathbf{E}_n is a diagonal matrix with 1 on its n -th diagonal element and 0 elsewhere.

Note that as R_k in (4) contains an expectation over the fading, the optimized precoders are independent of $\gamma_{l,k}$, and only depend on the angular information and variance β_k . Hence, we refer to this as a non-coherent joint transmission scenario and stress that no phase-synchronization is needed across SATs to achieve the considered rate. R_k does not have an analytical form, which makes problem (5) difficult to handle. In the following, we will develop an approximate expression for (4) to reformulate problem (5).

C. Problem Reformulation

As the first step to solve (5), we seek to reformulate the objective function in a more tractable form. To this end, we adopt an approximation to simplify the expression for the achievable SE. For positive definite matrices \mathbf{X} and \mathbf{Y} , it holds that

$$\mathbb{E} \{ \log_2 |\mathbf{I} + \mathbf{X}\mathbf{Y}^{-1}| \} \approx \log_2 |\mathbf{I} + \mathbb{E}\{\mathbf{X}\} \mathbb{E}\{\mathbf{Y}\}^{-1}|. \quad (6)$$

Remark 1. *The approximation in (6) has been shown to be tight in scalar cases [25]. However, to the best of our knowledge, there is no mathematical proof establishing its tightness in the matrix-valued case, although it has been used in that form in prior works, e.g., [26]. Our numerical evaluations indicated that the approximation tightness can vary; nevertheless, across all tested setups, the right-hand side (RHS) provided a reasonable approximation to the left-hand side (LHS) that is suitable for optimization. Section V offers a detailed numerical comparison of the LHS and RHS of (6) for SE evaluations.*

The SE expression can be simplified using (6). In particular,

$$R_k = \mathbb{E} \left\{ \log_2 \left| \mathbf{I}_M + \left(\sum_{l=1}^L \mathbf{H}_{l,k} \mathbf{W}_{l,k} \right) \left(\sum_{l=1}^L \mathbf{H}_{l,k} \mathbf{W}_{l,k} \right)^H \left(\sum_{i=1, i \neq k}^K \left(\sum_{l=1}^L \mathbf{H}_{l,k} \mathbf{W}_{l,i} \right) \left(\sum_{l=1}^L \mathbf{H}_{l,k} \mathbf{W}_{l,i} \right)^H + \sigma^2 \mathbf{I}_M \right)^{-1} \right| \right\} \quad (4)$$

for the signal term we have

$$\begin{aligned} & \mathbb{E} \left\{ \left(\sum_{l=1}^L \mathbf{H}_{l,k} \mathbf{W}_{l,k} \right) \left(\sum_{l=1}^L \mathbf{H}_{l,k} \mathbf{W}_{l,k} \right)^H \right\} \\ &= \mathbb{E} \left\{ \sum_{l=1}^L |\gamma_{l,k}|^2 \mathbf{b}_{l,k} \mathbf{a}_{l,k}^T \mathbf{W}_{l,k} \mathbf{W}_{l,k}^H \mathbf{a}_{l,k}^* \mathbf{b}_{l,k}^H \right\} \\ &= \sum_{l=1}^L \mathbb{E} \{ |\gamma_{l,k}|^2 \} \mathbf{b}_{l,k} \mathbf{a}_{l,k}^T \mathbf{W}_{l,k} \mathbf{W}_{l,k}^H \mathbf{a}_{l,k}^* \mathbf{b}_{l,k}^H \\ &= \sum_{l=1}^L \beta_{l,k} \mathbf{b}_{l,k} \mathbf{a}_{l,k}^T \mathbf{W}_{l,k} \mathbf{W}_{l,k}^H \mathbf{a}_{l,k}^* \mathbf{b}_{l,k}^H, \end{aligned} \quad (7)$$

where we use the notations $\mathbf{b}_{l,k} = \mathbf{b}_k(\theta_{l,k})$ and $\mathbf{a}_{l,k} = \mathbf{a}_k(\varphi_{l,k})$. For the interference-plus-noise term, we obtain

$$\begin{aligned} & \mathbb{E} \left\{ \sum_{i=1, i \neq k}^K \left(\sum_{l=1}^L \mathbf{H}_{l,k} \mathbf{W}_{l,i} \right) \left(\sum_{l=1}^L \mathbf{H}_{l,k} \mathbf{W}_{l,i} \right)^H + \sigma^2 \mathbf{I}_M \right\} \\ &= \sum_{i=1, i \neq k}^K \sum_{l=1}^L \beta_{l,k} \mathbf{b}_{l,k} \mathbf{a}_{l,k}^T \mathbf{W}_{l,i} \mathbf{W}_{l,i}^H \mathbf{a}_{l,k}^* \mathbf{b}_{l,k}^H + \sigma^2 \mathbf{I}_M. \end{aligned} \quad (8)$$

Therefore, the SE expression R_k in (4) can be approximated as \bar{R}_k in (9), shown at the top of the next page.

The sum SE maximization problem is thus reformulated as

$$\begin{aligned} & \text{maximize}_{\{\mathbf{W}_{l,k}\}_{\forall l,k}} \sum_{k=1}^K \bar{R}_k, \quad (10a) \\ & \text{subject to} \sum_{k=1}^K \text{Tr}(\mathbf{W}_{l,k}^H \mathbf{A}_{l,x} \mathbf{W}_{l,k}) \leq \rho_{l,x}, \quad \forall l, x = 1, \dots, X_l. \end{aligned} \quad (10b)$$

In the following, we first focus on the joint transmission mode considered in problem (10), which assumes full message sharing across SATs. We then extend the proposed framework to a mode with lower fronthaul overhead that reduces the message sharing requirement by restricting each stream to be transmitted by a single SAT through a stream-SAT association.

III. PRECODING DESIGN FOR NON-COHERENT JOINT TRANSMISSION

Problem (10) is non-convex due to the non-concavity of the objective function and the coupling between the precoding matrices. Weighted minimum mean square error (WMMSE) framework is a well-established approach for solving non-convex sum SE maximization problems involving interference terms [23]. In this section, we follow the WMMSE approach and tailor it to problem (10) by accommodating multiple general convex per-SAT power constraints. Since the reformulated problem (10) is based on the approximate SE

expression in (9), which depends on the channel only through the deterministic effective matrices $\tilde{\mathbf{H}}_{l,k} = \sqrt{\beta_{l,k}} \mathbf{b}_{l,k} \mathbf{a}_{l,k}^T$, we henceforth perform the derivations using the corresponding effective received signal obtained from (1) by replacing $\mathbf{H}_{l,k}$ with $\tilde{\mathbf{H}}_{l,k}$. This yields

$$\tilde{\mathbf{y}}_k = \sum_{l=1}^L \tilde{\mathbf{H}}_{l,k} \mathbf{W}_{l,k} \mathbf{x}_k + \sum_{i=1, i \neq k}^K \sum_{l=1}^L \tilde{\mathbf{H}}_{l,k} \mathbf{W}_{l,i} \mathbf{x}_i + \mathbf{n}_k. \quad (11)$$

Assuming that UE k uses the receive combining matrix $\mathbf{U}_k \in \mathbb{C}^{M \times S}$ to decode its desired signal, the estimated signal at UE k is given by $\hat{\mathbf{x}}_k = \mathbf{U}_k^H \tilde{\mathbf{y}}_k$. The MSE matrix for UE k can be expressed as

$$\begin{aligned} \mathbf{E}_k &= \mathbb{E} \{ (\hat{\mathbf{x}}_k - \mathbf{x}_k)(\hat{\mathbf{x}}_k - \mathbf{x}_k)^H \} = \\ & \mathbf{U}_k^H \left(\sum_{i=1}^K \sum_{l=1}^L \tilde{\mathbf{H}}_{l,k} \mathbf{W}_{l,i} \mathbf{W}_{l,i}^H \tilde{\mathbf{H}}_{l,k}^H \right) \mathbf{U}_k \\ & - 2\Re \left(\mathbf{U}_k^H \sum_{l=1}^L \tilde{\mathbf{H}}_{l,k} \mathbf{W}_{l,k} \right) + \sigma^2 \mathbf{U}_k^H \mathbf{U}_k + \mathbf{I}_S. \end{aligned} \quad (12)$$

The sum SE maximization problem in (10) can now be formulated as an equivalent weighted sum MSE minimization problem following the approach from [23]. Specifically, letting $\mathbf{C}_k \in \mathbb{C}^{S \times S}$ be a weight matrix associated with \mathbf{E}_k , we can solve the following problem instead of (10):

$$\begin{aligned} & \text{minimize}_{\{\mathbf{U}_k\}_{\forall k}, \{\mathbf{C}_k\}_{\forall k}, \{\mathbf{W}_{l,k}\}_{\forall l,k}} \sum_{k=1}^K \text{Tr}(\mathbf{C}_k \mathbf{E}_k) - \log_2 |\mathbf{C}_k|, \quad (13a) \\ & \text{subject to} \sum_{k=1}^K \text{Tr}(\mathbf{W}_{l,k}^H \mathbf{A}_{l,x} \mathbf{W}_{l,k}) \leq \rho_{l,x}, \quad \forall l, x = 1, \dots, X_l. \end{aligned} \quad (13b)$$

Problem (13) is equivalent to problem (10) in the sense that the optimal precoding matrices $\{\mathbf{W}_{l,k}\}$ are the same for both problems. Yet, (13) is more tractable than (10) as it is convex with respect to each block of variables, i.e., $\{\mathbf{U}_k\}$, $\{\mathbf{C}_k\}$, and $\{\mathbf{W}_{l,k}\}$. This motivates the use of the block coordinate descent method since the per-block convexity ensures convergence to a stationary point [27].

Assuming fixed $\{\mathbf{W}_{l,k}\}$, the optimal receive combining matrix can be readily obtained by setting $\frac{\partial \text{Tr}(\mathbf{E}_k)}{\partial \mathbf{U}_k} = \mathbf{0}$ for each individual UE. This results in

$$\mathbf{U}_k^* = \left(\sum_{i=1}^K \sum_{l=1}^L \tilde{\mathbf{H}}_{l,k} \mathbf{W}_{l,i} \mathbf{W}_{l,i}^H \tilde{\mathbf{H}}_{l,k}^H + \sigma^2 \mathbf{I}_M \right)^{-1} \tilde{\mathbf{H}}_k \mathbf{W}_i. \quad (14)$$

Then, assuming $\{\mathbf{U}_k\}$ and $\{\mathbf{W}_{l,k}\}$ are fixed, the optimal weight matrix \mathbf{C}_k can be found by solving $\frac{\partial (\text{Tr}(\mathbf{C}_k \mathbf{E}_k - \log_2 |\mathbf{C}_k|))}{\partial \mathbf{C}_k} = \mathbf{0}$ for \mathbf{C}_k , resulting in

$$\mathbf{C}_k^* = \frac{1}{\ln 2} \mathbf{E}_k^{-1}, \quad (15)$$

$$\bar{R}_k = \log_2 \left| \mathbf{I}_M + \left(\sum_{l=1}^L \beta_{l,k} \mathbf{b}_{l,k} \mathbf{a}_{l,k}^T \mathbf{W}_{l,k} \mathbf{W}_{l,k}^H \mathbf{a}_{l,k}^* \mathbf{b}_{l,k}^H \right) \left(\sum_{i=1, i \neq k}^K \sum_{l=1}^L \beta_{l,i} \mathbf{b}_{l,i} \mathbf{a}_{l,i}^T \mathbf{W}_{l,i} \mathbf{W}_{l,i}^H \mathbf{a}_{l,i}^* \mathbf{b}_{l,i}^H + \sigma^2 \mathbf{I}_M \right)^{-1} \right| \quad (9)$$

where \mathbf{E}_k is obtained from (12) after substituting \mathbf{U}_k^* . The final step is to optimize $\{\mathbf{W}_{l,k}\}$, which can be decomposed into L sub-problems with the l -th sub-problem being

$$\begin{aligned} & \text{minimize}_{\{\mathbf{W}_{l,k}\}_{\forall l,k}} \sum_{k=1}^K \text{Tr} \left(\sum_{i=1}^K \mathbf{C}_i \mathbf{U}_i^H \tilde{\mathbf{H}}_{l,i} \mathbf{W}_{l,k} \mathbf{W}_{l,k}^H \tilde{\mathbf{H}}_{l,i}^H \mathbf{U}_i \right. \\ & \left. - 2\mathbf{C}_k \Re \left(\mathbf{U}_k^H \tilde{\mathbf{H}}_{l,k} \mathbf{W}_{l,k} \right) \right), \end{aligned} \quad (16a)$$

$$\text{subject to } \sum_{k=1}^K \text{Tr} \left(\mathbf{W}_{l,k}^H \mathbf{A}_{l,x} \mathbf{W}_{l,k} \right) \leq \rho_{l,x}, \quad x = 1, \dots, X_l. \quad (16b)$$

We can now utilize the method of Lagrange multipliers to solve (16). Specifically, the Lagrangian is given by

$$\begin{aligned} \mathcal{L}_l = & \sum_{k=1}^K \text{Tr} \left(\mathbf{W}_{l,k}^H \left(\sum_{i=1}^K \tilde{\mathbf{H}}_{l,i}^H \mathbf{U}_i \mathbf{C}_i \mathbf{U}_i^H \tilde{\mathbf{H}}_{l,i} \right) \mathbf{W}_{l,k} - \right. \\ & \left. 2\mathbf{C}_k \Re \left(\mathbf{U}_k^H \tilde{\mathbf{H}}_{l,k} \mathbf{W}_{l,k} \right) \right) \\ & + \sum_{x=1}^{X_l} \left(\mu_{l,x} \left(\sum_{k=1}^K \text{Tr} \left(\mathbf{W}_{l,k}^H \mathbf{A}_{l,x} \mathbf{W}_{l,k} \right) - \rho_{l,x} \right) \right), \end{aligned} \quad (17)$$

where $\mu_{l,x}$ is the Lagrange multiplier associated with the x -th power constraint at SAT l . We need to solve the following problem

$$\text{minimize}_{\{\mathbf{W}_{l,k}\}_{\forall k}} \mathcal{L}_l, \quad (18)$$

which can be separately solved for the K UEs by setting $\frac{\partial \mathcal{L}_l}{\partial \mathbf{W}_{l,k}} = \mathbf{0}$. The optimal $\mathbf{W}_{l,k}$ for given $\boldsymbol{\mu}_l = [\mu_{l,1}, \dots, \mu_{l,X_l}]^T$ is obtained as

$$\begin{aligned} \mathbf{W}_{l,k}^* (\boldsymbol{\mu}_l) = & \left(\sum_{i=1}^K \tilde{\mathbf{H}}_{l,i}^H \mathbf{U}_i \mathbf{C}_i \mathbf{U}_i^H \tilde{\mathbf{H}}_{l,i} + \sum_{x=1}^{X_l} \mu_{l,x} \mathbf{A}_{l,x} \right)^{-1} \tilde{\mathbf{H}}_{l,k}^H \mathbf{U}_k \mathbf{C}_k. \end{aligned} \quad (19)$$

To obtain the optimal Lagrange multiplier vector $\boldsymbol{\mu}_l^*$, we first examine $\boldsymbol{\mu}_l = \mathbf{0}$. If the precoder $\mathbf{W}_{l,k}^*(\mathbf{0})$ computed from (19) satisfies all power constraints in (16b), then $\boldsymbol{\mu}_l^* = \mathbf{0}$. Otherwise, we update $\boldsymbol{\mu}_l$ using the ellipsoid method [28]. Specifically, we first identify a feasible upper-bound vector $\bar{\boldsymbol{\mu}}_l$ by geometric expansion: starting from $\boldsymbol{\mu}_l \succ \mathbf{0}$, we set $\boldsymbol{\mu}_l \leftarrow \alpha \boldsymbol{\mu}_l$ ($\alpha > 1$) and recompute (19) until all constraints in (16b) are met. We initialize an ellipsoid that contains the

box $[\mathbf{0}, \bar{\boldsymbol{\mu}}_l]$. Then, at iteration t , we compute $\mathbf{W}_{l,k}^*(\boldsymbol{\mu}_l^{(t)})$ from (19) and evaluate the residuals

$$\begin{aligned} g_{l,x}(\boldsymbol{\mu}_l^{(t)}) = & \sum_{k=1}^K \text{Tr} \left(\mathbf{W}_{l,k}^H(\boldsymbol{\mu}_l^{(t)}) \mathbf{A}_{l,x} \mathbf{W}_{l,k}(\boldsymbol{\mu}_l^{(t)}) \right) - \rho_{l,x}, \quad x = 1, \dots, X_l, \end{aligned} \quad (20)$$

where $\boldsymbol{\mu}_l^{(t)}$ is the center of the current ellipsoid. We then generate a cutting plane through the ellipsoid center using the residual vector $\mathbf{g}_l^{(t)} = [g_{l,1}(\boldsymbol{\mu}_l^{(t)}), \dots, g_{l,X_l}(\boldsymbol{\mu}_l^{(t)})]^T$ as the cut direction. Next, we apply a central-cut ellipsoid update: the ellipsoid is shrunk and its center is shifted opposite to the normalized cut direction. This procedure is repeated until the residuals are within the tolerance and the ellipsoid becomes sufficiently small.

The proposed precoding design is summarized in Algorithm 1 and the ellipsoid method for updating Lagrange multipliers is provided in Algorithm 2. The precoding matrices in Algorithm 1 are initialized using MMSE precoder as

$$\mathbf{W}_{l,k} = \sqrt{\bar{\rho}_{l,k}} \frac{\tilde{\mathbf{W}}_{l,k}}{\|\tilde{\mathbf{W}}_{l,k}\|_F}, \quad (21)$$

with $\tilde{\mathbf{W}}_{l,k} = \left(\sum_{i=1}^K \tilde{\mathbf{H}}_{l,i}^H \tilde{\mathbf{H}}_{l,i} + \sigma^2 \mathbf{I}_N \right)^{-1} \tilde{\mathbf{H}}_{l,k}^H \mathbf{Q}_{l,k}^{(S)}$ where $\mathbf{Q}_{l,k}^{(S)}$ is the matrix collecting the S dominant left singular vectors of $\tilde{\mathbf{H}}_{l,k}$, and $\bar{\rho}_{l,k} = \bar{\rho}_l \frac{\sqrt{\beta_{l,k}}}{\sum_{i=1}^K \sqrt{\beta_{l,i}}}$ where $\bar{\rho}_l = \min_x \rho_{l,x}$. Since each subproblem in Algorithm 1 is solved optimally, the objective value of (13) is non-increasing at every iteration and, being bounded below, the algorithm converges to a stationary point after a few iterations [23].

IV. FRONTHAUL-AWARE STREAMWISE TRANSMISSION WITH LIMITED MESSAGE SHARING

In Section III, we studied a joint transmission model where each UE is served by all SATs and SAT l applies a full precoding matrix $\mathbf{W}_{l,k}$ to potentially transmit all S streams to UE k . This approach requires distributing all S data streams of each UE to all SATs. In practice, such full message sharing can be challenging in LEO networks because the same data must be transferred from the ground to multiple SATs, either through multiple dedicated links from ground stations or through inter-satellite links. In either case, this imposes additional requirements on fronthaul capacity, as well as on latency and onboard processing constraints. Motivated by these practical limitations, we next propose a reduced-overhead scheme in which each of the S streams intended for UE k is transmitted by only one SAT. In this section, we consider the per-SAT total power constraints as a special case of the general power constraints studied in Section III.

Algorithm 1: Proposed Precoding Design under General Convex Power Constraints

- Inputs:** $\varphi_{l,k}, \theta_{k,l}, \beta_{l,k} \forall l, k, \sigma^2, \{\mathbf{A}_{l,x}, \rho_{l,x}\}_{x=1}^{X_l} \forall l, \epsilon, I_{\max}$.
- 1: Initialize the precoding matrices $\mathbf{W}_{l,k} \forall l, k$.
 - 2: Initialize $\delta = \epsilon + 1$ and set the initial value of the objective function in (13a) to $+\infty$.
 - 3: Set $I = 0$.
 - 4: **while** $\delta > \epsilon$ & $I < I_{\max}$ **do**
 - 5: $I \leftarrow I + 1$.
 - 6: Find receive combining matrices $\mathbf{U}_k^* \forall k$ from (14).
 - 7: Find weight matrices $\mathbf{C}_k^* \forall k$ from (15).
 - 8: For each SAT l , obtain $\boldsymbol{\mu}_l^* = [\mu_{l,1}^*, \dots, \mu_{l,X_l}^*]^\top$ via Algorithm 2.
 - 9: Update the precoding matrices $\mathbf{W}_{l,k}^*(\boldsymbol{\mu}_l^*) \forall l, k$ using (19).
 - 10: Compute the objective function in (13a) with the updated variables.
 - 11: Set δ as the difference between the current and previous objective function values.
 - 12: **end while**
- Output:** $\mathbf{W}_{l,k}^*(\boldsymbol{\mu}_l^*) \forall l, k$.
-

A. Precoding Design

Let $x_{k,s}$ be the s -th stream intended for UE k with unit power (i.e., the s -th entry of \mathbf{x}_k) and denote by $\pi_k(s)$ the index of the SAT that transmits the s -th stream of UE k . Furthermore, denote by $\mathbf{w}_{\pi_k(s),k,s} \in \mathbb{C}^N$ the precoding vector for the s -th stream of UE k applied by SAT $\pi_k(s)$. The effective received signal at UE k in this case is

$$\tilde{\mathbf{y}}_k = \sum_{i=1}^K \sum_{s=1}^S \tilde{\mathbf{H}}_{\pi_i(s),k} \mathbf{w}_{\pi_i(s),i,s} x_{i,s} + \mathbf{n}_k. \quad (22)$$

With the received signal model in (22) and applying the linear combiner \mathbf{U}_k to form $\hat{\mathbf{x}}_k = \mathbf{U}_k^H \tilde{\mathbf{y}}_k$, the MSE matrix becomes

$$\begin{aligned} \mathbf{E}_k &= \mathbb{E} \{ (\hat{\mathbf{x}}_k - \mathbf{x}_k) (\hat{\mathbf{x}}_k - \mathbf{x}_k)^H \} = \\ & \mathbf{U}_k^H \left(\sum_{i=1}^K \sum_{s=1}^S \tilde{\mathbf{H}}_{\pi_i(s),k} \mathbf{w}_{\pi_i(s),i,s} \mathbf{w}_{\pi_i(s),i,s}^H \tilde{\mathbf{H}}_{\pi_i(s),k}^H \right) \mathbf{U}_k \\ & - 2\Re(\mathbf{U}_k^H \mathbf{G}_k) + \sigma^2 \mathbf{U}_k^H \mathbf{U}_k + \mathbf{I}_S, \end{aligned} \quad (23)$$

where the desired effective channel matrix for UE k is

$$\mathbf{G}_k \triangleq \left[\tilde{\mathbf{H}}_{\pi_k(1),k} \mathbf{w}_{\pi_k(1),k,1}, \dots, \tilde{\mathbf{H}}_{\pi_k(S),k} \mathbf{w}_{\pi_k(S),k,S} \right] \in \mathbb{C}^{M \times S}. \quad (24)$$

Following the same steps as in Section III to cast the sum SE maximization problem as a weighted sum MSE minimization problem and applying block coordinate descent, the optimal receive combining vector and weight matrix can be obtained as

$$\mathbf{U}_k^* = \mathbf{J}_k^{-1} \mathbf{G}_k, \quad (25)$$

$$\mathbf{C}_k^* = \frac{1}{\ln 2} \mathbf{E}_k^{-1}, \quad (26)$$

Algorithm 2: Ellipsoid Method for Lagrange Multipliers Update (SAT l)

- Inputs:** $\tilde{\mathbf{H}}_{l,k}, \mathbf{U}_k, \mathbf{C}_k \forall k, \{\mathbf{A}_{l,x}, \rho_{l,x}\}_{x=1}^{X_l}, \alpha > 1, \epsilon, I_{\text{ell}}$.
- Initialization:**
- 1: Set $d = X_l$ (dimension of $\boldsymbol{\mu}_l$) and $\boldsymbol{\mu}_l = \mathbf{0}$.
 - 2: Compute $\mathbf{W}_{l,k}^*(\boldsymbol{\mu}_l) \forall k$ from (19) and the residuals $g_{l,x}(\boldsymbol{\mu}_l) \forall x$ from (20).
 - 3: **if** $g_{l,x}(\boldsymbol{\mu}_l) \leq 0$ for all $x = 1, \dots, d$ **then**
 - 4: **return** $\boldsymbol{\mu}_l^* = \mathbf{0}$.
 - 5: **end if**
 - 6: Choose an initial vector $\boldsymbol{\mu}_l^{(0)} \succ \mathbf{0}$.
 - 7: **while** $\exists x$ such that $g_{l,x}(\boldsymbol{\mu}_l^{(0)}) > 0$ **do**
 - 8: $\boldsymbol{\mu}_l^{(0)} \leftarrow \alpha \boldsymbol{\mu}_l^{(0)}$ (geometric expansion)
 - 9: Recompute $\mathbf{W}_{l,k}^*(\boldsymbol{\mu}_l^{(0)}) \forall k$ from (19) and $g_{l,x}(\boldsymbol{\mu}_l^{(0)}) \forall x$ from (20).
 - 10: **end while**
 - 11: Set $\bar{\boldsymbol{\mu}}_l = \boldsymbol{\mu}_l^{(0)}$ (feasible upper bound).
 - 12: $\mathbf{c}^{(0)} = \bar{\boldsymbol{\mu}}_l / 2, \mathbf{P}^{(0)} = \frac{d}{4} \text{diag}(\bar{\boldsymbol{\mu}}_l \odot \bar{\boldsymbol{\mu}}_l)$.
 - 13: Initialize an ellipsoid containing the box $[\mathbf{0}, \bar{\boldsymbol{\mu}}_l]$: $\mathcal{E}^{(0)} = \{ \boldsymbol{\mu} : (\boldsymbol{\mu} - \mathbf{c}^{(0)})^\top (\mathbf{P}^{(0)})^{-1} (\boldsymbol{\mu} - \mathbf{c}^{(0)}) \leq 1 \}$.
- Ellipsoid iterations:**
- 14: **for** $t = 0, 1, \dots, I_{\text{ell}} - 1$ **do**
 - 15: Set $\boldsymbol{\mu}_l^{(t)} = \mathbf{c}^{(t)}$ and compute $\mathbf{W}_{l,k}^*(\boldsymbol{\mu}_l^{(t)}) \forall k$ from (19).
 - 16: Compute residual vector $\mathbf{g}_l^{(t)} = [g_{l,1}(\boldsymbol{\mu}_l^{(t)}), \dots, g_{l,d}(\boldsymbol{\mu}_l^{(t)})]^\top$ using (20).
 - 17: **if** $\max_x g_{l,x}(\boldsymbol{\mu}_l^{(t)}) \leq \epsilon$ & $\max_i \sqrt{\mathbf{P}^{(t)}(i,i)} \leq \epsilon$ **then**
 - 18: **break**
 - 19: **end if**
 - 20: Set cut normal $\mathbf{s}^{(t)} = \mathbf{g}_l^{(t)}$.
 - 21: Normalize: $\tilde{\mathbf{s}}^{(t)} = \frac{\mathbf{P}^{(t)} \mathbf{s}^{(t)}}{\sqrt{(\mathbf{s}^{(t)})^\top \mathbf{P}^{(t)} \mathbf{s}^{(t)}}}$.
 - 22: Update center (central cut):
 - 23: $\mathbf{c}^{(t+1)} = \mathbf{c}^{(t)} - \frac{1}{d+1} \tilde{\mathbf{s}}^{(t)}$.
 - 24: Enforce non-negativity: $\mathbf{c}^{(t+1)} \leftarrow [\mathbf{c}^{(t+1)}]_+$.
 - 25: Update shape matrix:
 - 26: $\mathbf{P}^{(t+1)} = \frac{d^2}{d^2 - 1} \left(\mathbf{P}^{(t)} - \frac{2}{d+1} \tilde{\mathbf{s}}^{(t)} (\tilde{\mathbf{s}}^{(t)})^\top \right)$.
 - 27: **end for**
- Output:** $\boldsymbol{\mu}_l^* = \mathbf{c}^{(t)}$.
-

where

$$\mathbf{J}_k \triangleq \sum_{i=1}^K \sum_{s=1}^S \tilde{\mathbf{H}}_{\pi_i(s),k} \mathbf{w}_{\pi_i(s),i,s} \mathbf{w}_{\pi_i(s),i,s}^H \tilde{\mathbf{H}}_{\pi_i(s),k}^H + \sigma^2 \mathbf{I}_M. \quad (27)$$

Next, we need to optimize the precoding vectors having fixed $\{\mathbf{U}_k\}$ and $\{\mathbf{C}_k\}$. The corresponding optimization problem is

$$\text{minimize}_{\{\mathbf{w}_{l,k,s}\}_{(k,s) \in \mathcal{T}_l}} \sum_{k=1}^K \text{Tr}(\mathbf{C}_k \mathbf{E}_k), \quad (28a)$$

$$\text{subject to} \sum_{(k,s) \in \mathcal{T}_l} \|\mathbf{w}_{l,k,s}\|^2 \leq \rho_l, \forall l, \quad (28b)$$

where $\mathcal{T}_l \triangleq \{(k, s) : \pi_k(s) = l\}$ and ρ_l denotes the maximum transmit power for SAT l . After some mathematical manipulations, problem (28) can be decoupled into L independent sub-problems, each corresponding to precoding optimization for a particular SAT. The l -th sub-problem can be expressed as

$$\underset{\{\mathbf{w}_{l,k,s}\}_{(k,s) \in \mathcal{T}_l}}{\text{minimize}} \sum_{(i,s) \in \mathcal{T}_l} (\mathbf{w}_{l,k,s}^H \mathbf{T}_l \mathbf{w}_{l,k,s} - 2\Re(\mathbf{z}_{k,l,s}^H \mathbf{w}_{l,k,s})), \quad (29a)$$

$$\text{subject to} \sum_{(k,s) \in \mathcal{T}_l} \|\mathbf{w}_{l,k,s}\|^2 \leq \rho_l, \quad \forall l, \quad (29b)$$

with

$$\mathbf{T}_l \triangleq \sum_{i=1}^K \tilde{\mathbf{H}}_{l,i}^H \mathbf{U}_i \mathbf{C}_i \mathbf{U}_i^H \tilde{\mathbf{H}}_{l,i} \quad (30)$$

$$\mathbf{z}_{k,l,s} \triangleq \tilde{\mathbf{H}}_{l,k}^H \mathbf{U}_k \mathbf{C}_k \mathbf{e}_s, \quad (31)$$

where \mathbf{e}_s is the s -th standard basis vector in \mathbb{C}^S . Applying the Lagrange multiplier approach, the solution to (29) can be obtained as

$$\mathbf{w}_{l,i,s}^*(\mu_l) = (\mathbf{T}_l + \mu_l \mathbf{I}_N)^{-1} \mathbf{z}_{i,l,s}, \quad (32)$$

where μ_l is the Lagrange multiplier associated with constraint (29b) and can be updated using the bisection method.

B. Streamwise Satellite Association

In the streamwise transmission scheme described in Section IV-A, the s -th stream of UE k is transmitted by only one SAT, indexed by $\pi_k(s)$, and this mapping determines which precoding vectors are active in the received signal model (22) and in the per-SAT assignment sets \mathcal{T}_l . In this subsection, we specify how to construct $\{\pi_k(s)\}_{s=1}^S$ for UE k .

Recall that the sCSI-based channel matrix from SAT l to UE k is $\tilde{\mathbf{H}}_{l,k} \in \mathbb{C}^{M \times N}$. For a given UE k , we form the aggregated sCSI-based channel by concatenating all L blocks:

$$\tilde{\mathbf{H}}_k \triangleq [\tilde{\mathbf{H}}_{1,k}, \tilde{\mathbf{H}}_{2,k}, \dots, \tilde{\mathbf{H}}_{L,k}] \in \mathbb{C}^{M \times (LN)}. \quad (33)$$

Since UE k has M antennas, $\tilde{\mathbf{H}}_k$ has at most M non-zero singular values (under the standard assumption that $LN \geq M$). Let the economy-size singular value decomposition (SVD) be

$$\tilde{\mathbf{H}}_k = \mathbf{Q}_k \Sigma_k \mathbf{V}_k^H, \quad (34)$$

and denote by $\mathbf{v}_{k,m}$ the m -th column of \mathbf{V}_k . This vector describes the m -th transmit-side eigenmode of UE k across the aggregated antenna array formed by all SATs. To perform the streamwise association, we first quantify how the energy of $\mathbf{v}_{k,m}$ is distributed across the L SATs' antenna arrays. In other words, we measure how much each SAT l contributes to the m -th eigenmode. To this end, we partition $\mathbf{v}_{k,m}$ into L consecutive blocks of length N , with each block corresponding to one SAT:

$$\mathbf{v}_{k,m} = [(\mathbf{v}_{k,m}^{(1)})^T, \dots, (\mathbf{v}_{k,m}^{(L)})^T]^T, \quad \mathbf{v}_{k,m}^{(l)} \in \mathbb{C}^N. \quad (35)$$

Since $\|\mathbf{v}_{k,m}\|^2 = 1$, we define the normalized contribution of SAT l to the m -th eigenmode as

$$\eta_{l,k,m} \triangleq \|\mathbf{v}_{k,m}^{(l)}\|^2, \quad l = 1, \dots, L, \quad m = 1, \dots, M, \quad (36)$$

which satisfies $\sum_{l=1}^L \eta_{l,k,m} = 1$ for every m . Hence, $\eta_{l,k,m}$ can be interpreted as a participation factor indicating how much of the m -th eigenmode is carried by the antennas of SAT l .

We intend to transmit $S \leq M$ streams over the S strongest eigenmodes of $\tilde{\mathbf{H}}_k$, and assign each of these eigenmodes/streams to a serving SAT. We next determine the stream-SAT association $\pi_k(s)$ by enforcing a one-to-one assignment between the S streams of UE k and S distinct SATs. To this end, we introduce the binary assignment variables $q_{l,k,s} \in \{0, 1\}$, where $q_{l,k,s} = 1$ indicates that SAT l is selected to transmit the s -th stream of UE k . Using the participation factors in (36), we compute the association for UE k 's streams by solving the following linear assignment problem:

$$\underset{\{q_{l,k,s}\}_{\forall l,s}}{\text{maximize}} \sum_{s=1}^S \sum_{l=1}^L \eta_{l,k,s} q_{l,k,s}, \quad (37a)$$

$$\text{subject to} \sum_{l=1}^L q_{l,k,s} = 1, \quad \forall s, \quad (37b)$$

$$\sum_{s=1}^S q_{l,k,s} \leq 1, \quad \forall l, \quad (37c)$$

$$q_{l,k,s} \in \{0, 1\}, \quad \forall l, s. \quad (37d)$$

Constraint (37b) ensures that each stream s is assigned to exactly one SAT, while (37c) ensures that each SAT is used for at most one stream of UE k , yielding S distinct serving SATs (assuming $L \geq S$). Problem (37) is a maximum-weight bipartite matching problem and can be solved efficiently by applying the Hungarian algorithm [29]. The resulting mapping is obtained as $\pi_k(s) = l$ if $q_{l,k,s} = 1$. In a nutshell, the mapping $\pi_k(s)$ decides which SAT is responsible for transmitting stream s to UE k , and stream s here corresponds to a specific UE spatial direction.

Once $\{\pi_k(s)\}$ are obtained, for all (l, k, s) with $l \neq \pi_k(s)$, the corresponding beamforming vector is zero. Consequently, each SAT l optimizes the subset of vectors indexed by $\mathcal{T}_l \triangleq \{(k, s) : \pi_k(s) = l\}$ in the precoder optimization problem (28).

The proposed streamwise association and precoding design are summarized in Algorithm 3. We initialize the precoding vectors as

$$\mathbf{w}_{l,k,s}^{(0)} = \sqrt{\bar{\rho}_{l,k,s}} \frac{\tilde{\mathbf{W}}_{l,k} \mathbf{e}_s}{\|\tilde{\mathbf{W}}_{l,k} \mathbf{e}_s\|}, \quad (38)$$

where $\bar{\rho}_{l,k,s} = \rho_l \frac{\sqrt{\beta_{l,k}}}{\sum_{(i,s') \in \mathcal{T}_l} \sqrt{\beta_{l,i}}}$ if $(k, s) \in \mathcal{T}_l$ and $\bar{\rho}_{l,k,s} = 0$ otherwise, and $\tilde{\mathbf{W}}_{l,k}$ is defined after (21).

To further illustrate how the participation factors $\{\eta_{l,k,m}\}$ describe the eigenmode structure of the aggregated channel $\tilde{\mathbf{H}}_k$, we consider a single-UE toy example with $M = 4$ antennas and $L = 4$ serving SATs. Recall that under the LoS channel model in (2), each SAT-UE link has the form $\tilde{\mathbf{H}}_{l,k} = \sqrt{\beta_{l,k}} \mathbf{b}(\theta_{l,k}) \mathbf{a}^T(\phi_{l,k})$, where $\mathbf{b}(\cdot)$ is the UE-side array response vector. For a half-wavelength ULA with $M = 4$, we have $\mathbf{b}(\theta) = [1, e^{j\pi \sin \theta}, e^{j2\pi \sin \theta}, e^{j3\pi \sin \theta}]^T$, and the

Algorithm 3: Streamwise SAT Association and Precoding Design

Inputs: $\varphi_{l,k}, \theta_{k,l}, \beta_{l,k} \forall l, k, \sigma^2, \rho_l \forall l, \alpha > 1, \epsilon, I_{\max}$.

- 1: Form the sCSI-based effective channel matrices
 $\tilde{\mathbf{H}}_{l,k} = \sqrt{\beta_{l,k}} \mathbf{b}_{l,k} \mathbf{a}_{l,k}^T \forall l, k$.
 - 2: **for** $k = 1, 2, \dots, K$ **do**
 - 3: Construct the aggregated channel $\tilde{\mathbf{H}}_k$ using (33).
 - 4: Compute the economy-size SVD $\tilde{\mathbf{H}}_k = \mathbf{Q}_k \Sigma_k \mathbf{V}_k^H$.
 - 5: **for** $m = 1, 2, \dots, M$ **do**
 - 6: Partition $\mathbf{v}_{k,m}$ into $\{\mathbf{v}_{k,m}^{(l)}\}_{l=1}^L$ as in (35).
 - 7: Compute $\eta_{l,k,m} = \|\mathbf{v}_{k,m}^{(l)}\|^2 \forall l$ as in (36).
 - 8: **end for**
 - 9: Solve the assignment problem (37) via the Hungarian algorithm to obtain $\{q_{l,k,s}\}$.
 - 10: Set $\pi_k(s) = l$ if $q_{l,k,s} = 1 \forall s$.
 - 11: **end for**
 - 12: Construct the per-SAT stream index sets
 $\mathcal{T}_l = \{(k, s) : \pi_k(s) = l\} \forall l$.
 - 13: Initialize $\mathbf{w}_{l,k,s} \forall l, k, s$.
 - 14: Initialize $\delta = \epsilon + 1$ and set the initial value of the objective function to $+\infty$.
 - 15: Set $I = 0$.
 - 16: **while** $\delta > \epsilon$ & $I < I_{\max}$ **do**
 - 17: $I \leftarrow I + 1$.
 - 18: Find receive combining matrices $\mathbf{U}_k^* \forall k$ from (25).
 - 19: Find weight matrices $\mathbf{C}_k^* \forall k$ from (26).
 - 20: For each SAT l , obtain μ_l^* using the bisection method.
 - 21: Update the precoding vectors $\mathbf{w}_{l,i,s}^*(\mu_l^*) \forall l, (i, s) \in \mathcal{T}_l$ using (32).
 - 22: Compute the objective value with the updated variables.
 - 23: Set δ as the difference between the current and previous objective values.
 - 24: **end while**
- Output:** Stream-SAT associations $\{\pi_k(s)\}$ and precoders $\{\mathbf{w}_{l,k,s}^*\}$.
-

inner product between two array response vectors can be written as

$$\mathbf{b}(\theta_i)^H \mathbf{b}(\theta_j) = \sum_{m=0}^{M-1} e^{j\pi n(\sin \theta_j - \sin \theta_i)}. \quad (39)$$

Hence, two links arriving from θ_i and θ_j are orthogonal on the UE side when $\Delta \triangleq \sin \theta_j - \sin \theta_i \in \{\pm 0.5, \pm 1, \pm 1.5\}$. Fig. 2 shows a case where the UE-side array response vectors of the four SAT-UE links are mutually orthogonal. This is obtained by selecting the AoAs such that $\sin \theta_{l,k} \in \{-0.9, -0.4, 0.1, 0.6\}$, for which all pairwise differences Δ belong to $\{\pm 0.5, \pm 1, \pm 1.5\}$. In this case, each SAT's energy is concentrated in a single eigenmode, with near-zero projection onto the other modes. Consequently, streamwise transmission is naturally aligned with the channel eigen-structure and is expected to perform close to joint transmission discussed in Section III, while reducing fronthaul load.

Fig. 3 shows a non-orthogonal case where the AoAs are set to $\theta_{l,k} \in \{-19.87^\circ, -6.84^\circ, 6.84^\circ, 19.87^\circ\}$ (equivalently,

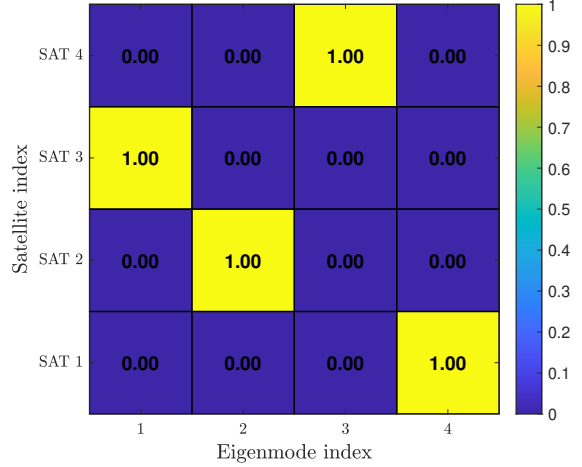


Fig. 2: Satellite participation factors of the aggregated channel eigenmodes when UE-side array responses are orthogonal. In this case, each SAT contributes essentially to one eigenmode and close to zero to the others.

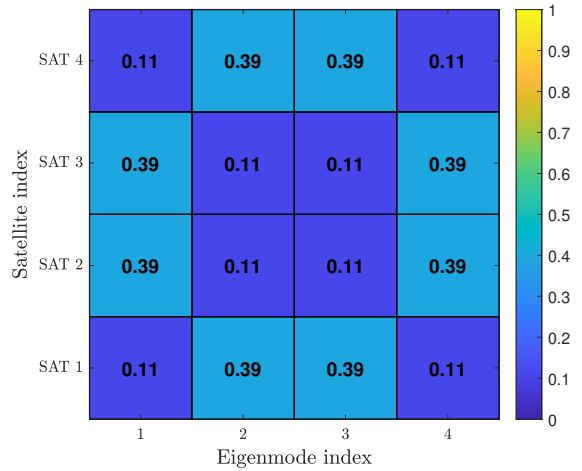


Fig. 3: Satellite participation factors of the aggregated channel eigenmodes when UE-side array responses are not orthogonal. In this case, the eigenmodes are shared across multiple SATs, so each SAT contributes to more than one eigenmode.

$\sin \theta_{l,k} \in \{-0.340, -0.119, 0.119, 0.340\}$), which does not satisfy the above orthogonality condition. Here, the eigenmodes are shared across multiple SATs and the participation factors are distributed across rows, indicating that streamwise transmission departs from joint transmission and may trade SE for reduced fronthaul load. We evaluate the SE impact in Section V.

Remark 2. The singular values of $\tilde{\mathbf{H}}_k$ in (34) quantify the strength of the spatial eigenmodes. If some of these eigenmodes are very weak, assigning a dedicated SAT and transmitting one stream over such a mode may be inefficient, since even the SAT with the largest participation factor $\eta_{l,k,m}$ yields only a small received signal power along that dimension. Accordingly, it may be preferable to transmit only over

the strongest modes. In such cases, when selecting a set of serving SATs for UE k , one may prioritize SATs that contribute strongly to the dominant eigenmodes by using an aggregate power-weighted score, for example

$$\bar{\eta}_{l,k} \triangleq \sum_{m=1}^M \bar{\sigma}_{k,m}^2 \eta_{l,k,m}, \quad (40)$$

where $\bar{\sigma}_{k,m}$ is the m -th singular value of $\tilde{\mathbf{H}}_k$. We can then select the SATs with the largest $\bar{\eta}_{l,k}$, followed by a stream-SAT assignment for the active eigenmodes. This favors SATs that are most relevant for the strong eigenmodes, thereby avoiding the allocation of resources to very weak spatial dimensions.

V. NUMERICAL RESULTS

In this section, we evaluate the performance of the proposed methods for joint and streamwise transmission in distributed LEO satellite communication networks. To reflect a realistic scenario, the simulation parameters are chosen to be consistent with publicly available FCC documentation, 3GPP technical report on non-terrestrial networks, and widely used assumptions in the literature for assessing Starlink systems [30]–[32].

Unless otherwise specified, the following parameters are used for simulations: We consider an orbital altitude of $h = 560$ km [30] with $L = 4$ visible SATs serving $K = 2$ UEs. Each SAT is equipped with $N = 64$ antennas and each UE has $M = 4$ antennas. Each UE is served with $S = 2$ streams. Communication takes place at the carrier frequency of $f_c = 20$ GHz with 400 MHz of bandwidth [31], and the noise power spectral density at the UEs is -174 dBm/Hz with a 1.2 dB noise figure [32]. For the azimuth angles, we select UE 1 as a reference; for each SAT l , the reference UE-side azimuth angles, $\theta_{l,1} \forall l$, are independently drawn from $\text{Uniform}[-90^\circ, 90^\circ]$ and the azimuth angles of UE 2, $\theta_{l,2} \forall l$, are generated by adding a small random drift to the reference angles, i.e., $\theta_{l,2} = \theta_{l,1} + \Delta\theta_l$, where $\Delta\theta_l \sim \text{Uniform}[-1^\circ, 1^\circ]$ and the result is clipped to $\text{Uniform}[-90^\circ, 90^\circ]$. The SAT-side azimuth angles, $\rho_{l,k}$, are generated using the same procedure. The large-scale fading coefficients are

$$\beta_{l,k} = G_u G_s \left(\frac{\nu_c}{4\pi f_c d_{l,k}} \right)^2, \forall l, k, \quad (41)$$

where $G_u = 8$ dBi and $G_s = 20$ dBi are the antenna gains of the UEs and the SATs, respectively, and $\nu_c = 3 \cdot 10^8$ is the speed of light. Furthermore, $d_{l,k}$ is the distance between SAT l and UE k , given by the slant range expression as

$$d_{l,k} = -R_E \sin(\vartheta_{l,k}) + \sqrt{(R_E + h)^2 - (R_E \cos(\vartheta_{l,k}))^2}, \quad (42)$$

where $R_E = 6371$ km is the Earth radius and $\vartheta_{l,k}$ is the elevation angle. Again, UE 1 is used as a reference and $\vartheta_{l,1} \forall l$ is drawn independently from $\text{Uniform}[20^\circ, 90^\circ]$. The elevation angles for UE 2 are then obtained by perturbing the reference values as $\vartheta_{l,2} = \vartheta_{l,1} + \Delta\vartheta_l$ with $\Delta\vartheta_l \sim \text{Uniform}[-0.5^\circ, 0.5^\circ]$, followed by clipping to the interval $[20^\circ, 90^\circ]$. The Rician factor is set as $\kappa_{l,k} = 12$ dB, $\forall l, k$. For the joint transmission scheme studied in Section III, we impose per-SAT power constraints. In the figures, ρ denotes

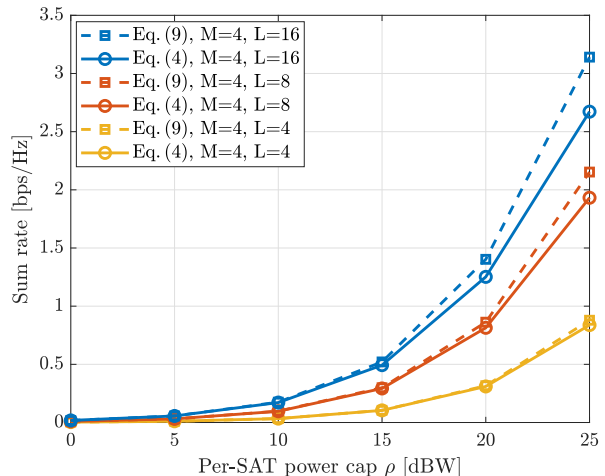


Fig. 4: Comparison between the exact and approximate SE expressions in (4) and (9), respectively.

the common power cap applied to each SAT. Finally, in implementing the iterative algorithms, the maximum number of iterations is set to $I_{\max} = 40$, and the convergence threshold to $\epsilon = 10^{-4}$.

Fig. 4 evaluates the approximation provided in (6) by comparing the SE values obtained from the exact SE expression in (4) and the approximated value in (9). To isolate the effect of the approximation from the proposed precoder design, MMSE precoding is employed, and the results are averaged over 10000 Monte Carlo simulations. Furthermore, the number of streams equals the number of UE antennas in this simulation, i.e., $S = M = 4$. For all cases, the two curves nearly overlap in the low-power regime, while the gap between them increases at high transmit powers. Further, the gap between the curves become larger with increasing L . This is because as L increases, both the desired signal power term and the corresponding interference term involve more SATs whose contributions fluctuate from realization to realization due to the independent random phases. Nevertheless, the two curves (exact and approximated ones) exhibit consistent trends with varying parameters. This supports the use of (9) as a tractable surrogate of (4) for precoder design and subsequent analysis. In the following simulations, all SE curves are obtained via Monte Carlo averaging of the exact SE in (4), while the approximation in (9) is used only to enable tractable precoder optimization.

Fig. 5 compares the SE of the joint transmission scheme studied in Section III with the streamwise transmission scheme presented in Section IV. In Fig. 5, the UE-side azimuth angles are chosen such that, for each UE, the four SAT-UE links generate approximately orthogonal UE-side array response vectors. As a result, the aggregated sCSI-based channel $\tilde{\mathbf{H}}_k$ exhibits an eigen-structure where each dominant UE spatial mode is carried almost entirely by one SAT. Therefore, joint transmission offers little additional gain from distributing a stream across multiple SATs, as can be observed from the figure.

Fig. 6 compares joint and streamwise transmissions in the

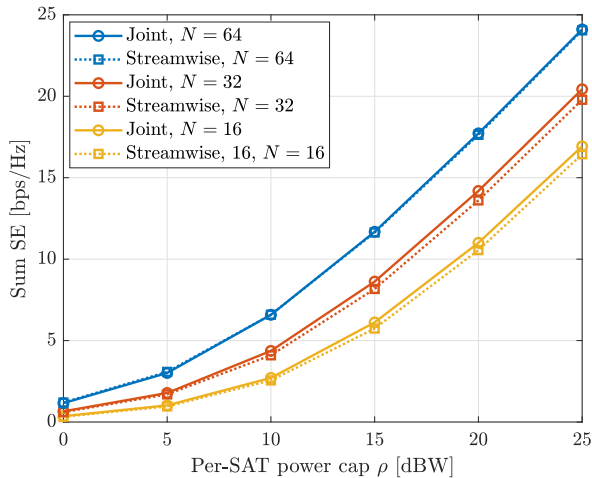


Fig. 5: Comparison of joint and streamwise transmissions under UE-side orthogonality.

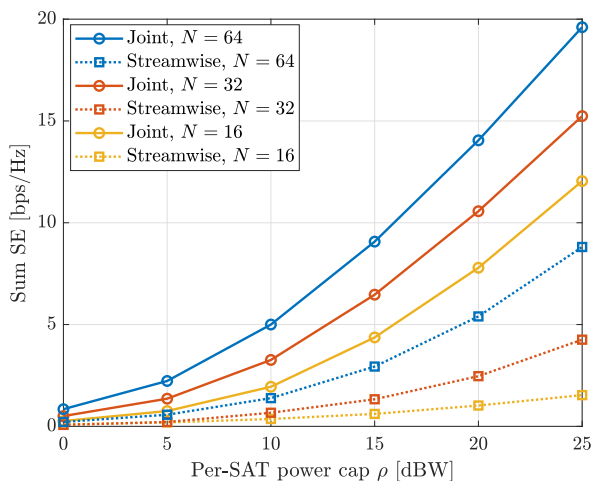


Fig. 6: Comparison of joint and streamwise transmissions when UE-side channels are non-orthogonal.

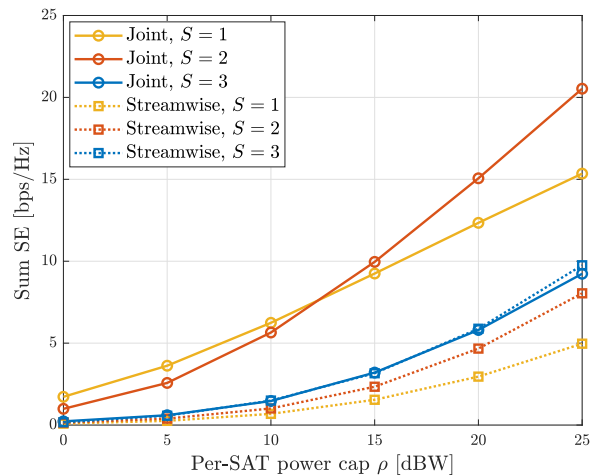
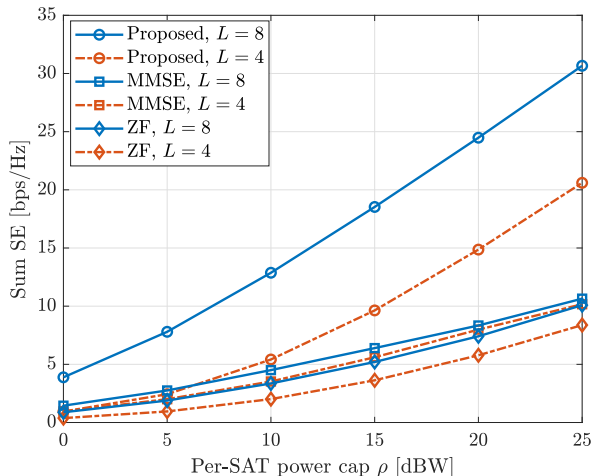


Fig. 7: Performance of joint and streamwise transmissions with different number of streams per UE.

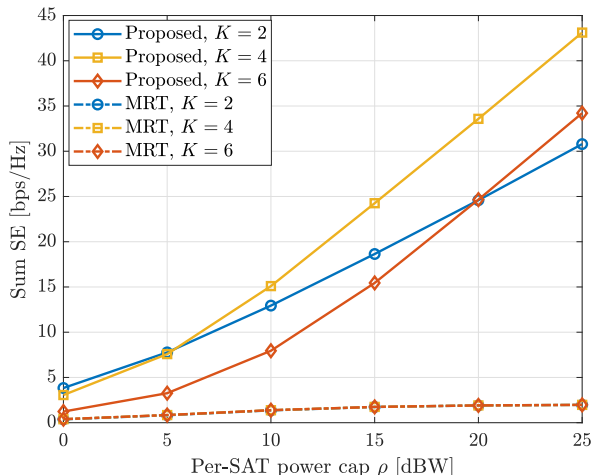
non-orthogonal setting, where the UE-side azimuth angles are randomly generated as described at the beginning of the section. In this case, the UE-side array response vectors associated with different SATs are correlated, so the SAT-UE channels are no longer separated into nearly orthogonal spatial subspaces. Hence, joint transmission can exploit the overlap between SAT links by distributing each stream across multiple SATs and choosing the weights to shape the transmitted signals to suppress interference. On the other hand, in streamwise transmission, each stream is radiated by a single SAT, which significantly limits the ability to manage interference. As a result, streamwise transmission becomes noticeably more interference-limited, while joint transmission retains additional degrees of freedom to balance signal enhancement and interference mitigation, leading to the large SE gap between the two schemes as observed in Fig. 6. Comparing Fig. 5 and Fig. 6, we conclude that when the UE-side channel subspaces are close to orthogonal, streamwise transmission is near-optimal and offers a low-overhead alternative to joint transmission. When the channels are not orthogonal, joint transmission provides significant SE gains, at the cost of higher fronthaul overhead.

Fig. 7 depicts the performance of the proposed joint and streamwise transmission modes for different numbers of streams per UE. For joint transmission, increasing the number of streams from $S = 1$ to $S = 2$ improves the sum SE, particularly at higher power budgets. However, further increasing to $S = 3$ degrades performance since inter-UE interference becomes dominant and a UE with $M = 4$ antennas has limited spatial degrees of freedom to suppress it. On the other hand, for streamwise transmission, increasing the number of streams from $S = 1$ to $S = 2$ and from $S = 2$ to $S = 3$ consistently improves performance as restricting each stream to a single SAT reduces the amount of interference compared to joint transmission. Another important observation is that, for the considered setup, joint and streamwise transmission achieve almost identical performance when $S = 3$ because the potential beamforming gain of joint transmission is largely offset by the resulting interference. Overall, these results highlight that the number of streams and the transmission mode should be selected jointly based on the system configuration.

Fig. 8 reports the achievable SE for the proposed joint precoding in Section III and classical baselines. Existing cooperative satellite precoding methods in [17]–[19], [21], [22], [33] target single-antenna ground UEs and thus, do not address the multi-antenna UE setting considered in this paper and their proposed approaches are not directly comparable with the joint precoding design presented in this paper. For this reason, we benchmark against the well-known MMSE, zero forcing (ZF), and maximum ratio transmission (MRT) precoders, implemented using the available sCSI-based channel model and then enforced to satisfy per-SAT power caps. We can see in Fig. 8(a) that the proposed joint transmission scheme notably outperforms MMSE and ZF benchmarks. That is because our method alternates between updating the transmit precoders, the receive combiners, and MSE weights. So, each iteration refines the beamformers toward directions that better suppress interference while keeping strong alignment with the



(a) Performance of the proposed scheme, MMSE precoding, and ZF precoding.



(b) Performance of the proposed scheme and an MRT baseline with orthogonal (e.g., TDMA) transmissions, where each UE is served by its closest SAT.

Fig. 8: Performance comparison between the proposed joint precoding and well-known benchmarks.

desired channels. Furthermore, increasing the number of SATs from $L = 4$ to $L = 8$ provides additional distributed transmit dimensions that our iterative joint design can actively exploit to reshape interference and redistribute each SAT's power across UEs/streams and spatial directions. Fig. 8(b) compares the proposed joint transmission scheme with an orthogonal MRT baseline where UEs are served in an orthogonal manner by only their closest SAT, which applies MRT precoding. We have $L = 8$ SATs and plot the results for $K = 2, 4, 6$ UEs. The MRT performance is poor because each UE is served by only a single SAT and the orthogonal scheduling incurs a $1/K$ penalty. For the proposed joint transmission, $K = 4$ outperforms $K = 2$ and $K = 6$. This is because increasing K from 2 to 4 enables spatial multiplexing of more UEs and thus increases the sum SE. At $K = 6$, the inter-UE interference become more pronounced, reducing the

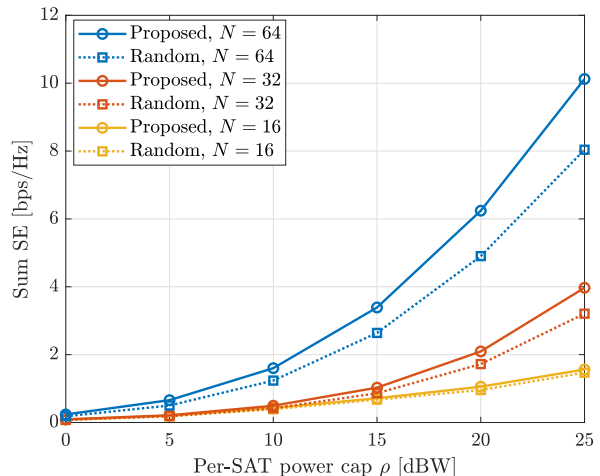


Fig. 9: Performance of streamwise transmission with the proposed association and a random association.

achievable gains. Hence, the number of simultaneously served UEs should be selected carefully for a given system dimension.

Finally, Fig. 9 evaluates the impact of stream-SAT association in the streamwise transmission studied in Section IV by comparing the proposed association strategy with a random baseline that randomly assigns SATs to UE eigenmodes when we have $L = 8$ SATs. Since streamwise transmission forces each stream to be carried by a single SAT, the association step directly determines whether a stream is transmitted by a SAT that has a strong projection onto that eigenmode or by a poorly matched SAT whose contribution is weak. The proposed strategy matches each eigenmode to a SAT that contributes strongly to it, yielding higher desired signal gain. The random strategy, however, ignores this structure, sometimes wasting power on weak stream-SAT pairings. Consequently, the proposed association achieves higher SEs than the random strategy and the gap becomes more pronounced as the per-SAT power cap increases, since the system gradually transitions from a noise-limited regime to an interference-limited regime. Furthermore, the gap between proposed and random association widens as the number of SAT antennas increases. As the number of SAT antennas N increases, the available array gain becomes larger, and the proposed association can better exploit it.

VI. CONCLUSIONS

This paper studied cell-free massive MIMO-inspired downlink transmission from multiple LEO satellites to multi-antenna ground users. Due to the limited availability of instantaneous CSI and the intractability of the exact ergodic SE, we adopted a tractable approximate SE expression that enables precoder design using only sCSI. We considered two multi-stream transmission strategies: joint non-coherent transmission, where each satellite transmits all user streams, and streamwise transmission, where each stream is transmitted by a single satellite. None of the strategies requires phase-synchronization across the satellites, in contrast to ground-based cell-free massive MIMO.

Our numerical results demonstrated that when the satellite-user links are close to orthogonal at the user (i.e., the user-side channel subspaces are well separated), streamwise transmission achieves nearly the same SE as joint transmission, since each dominant spatial mode is effectively carried by a single satellite and additional multi-satellite sharing provides little extra gain. Therefore, the same performance can be achieved with much lower fronthaul requirements. By contrast, in non-orthogonal channel conditions, joint transmission can better exploit multi-satellite interference shaping, and streamwise transmission exhibits a clear performance-overhead trade-off, sacrificing some SE in exchange for lower fronthaul overhead. Moreover, the numerical results indicated that the number of streams and the transmission mode must be selected jointly: when many streams are multiplexed and the users have limited spatial degrees of freedom for interference suppression, the beamforming gain of joint transmission is largely offset by the resulting inter-user interference, diminishing its advantage. Further, for a given system dimension, serving too many users simultaneously can make the system interference-limited and reduce the achievable gains; hence, the number of simultaneously served users should be chosen carefully.

REFERENCES

- [1] P. Ramezani and E. Björnson, "Cell-free MIMO in space: Cooperative satellite transmission with multi-antenna ground users," submitted to 2026 IEEE International Conference on Communications (ICC) Workshops.
- [2] ITU-R, "M. 2160: framework and overall objectives of the future development of IMT for 2030 and beyond," [Online]. Available: <https://www.itu.int/rec/R-REC-M.2160/en> 2023.
- [3] A. I. Perez-Neira, M. A. Vazquez, M. B. Shankar, S. Maleki, and S. Chatzinotas, "Signal processing for high-throughput satellites: Challenges in new interference-limited scenarios," *IEEE Signal Processing Magazine*, vol. 36, no. 4, pp. 112–131, 2019.
- [4] M. A. Jamshed *et al.*, "Non-terrestrial networks for 6G: Integrated, intelligent, and ubiquitous connectivity," *IEEE Communications Standards Magazine*, vol. 9, no. 3, pp. 86–93, 2025.
- [5] L. You *et al.*, "Ubiquitous integrated sensing and communications for massive MIMO LEO satellite systems," *IEEE Internet of Things Magazine*, vol. 7, no. 4, pp. 30–35, 2024.
- [6] D. Wu, C. Qin, Y. Cui, P. He, and R. Wang, "Space-ground multicast group control for multiuser LEO satellite networks," *IEEE Transactions on Wireless Communications*, vol. 23, no. 2, pp. 1622–1633, 2024.
- [7] X. Luo, H.-H. Chen, and Q. Guo, "LEO/VLEO satellite communications in 6G and beyond network technologies, applications, and challenges," *IEEE Network*, vol. 38, no. 5, pp. 273–285, 2024.
- [8] L. You *et al.*, "Massive MIMO transmission for LEO satellite communications," *IEEE Journal on Selected Areas in Communications*, vol. 38, no. 8, pp. 1851–1865, 2020.
- [9] —, "Hybrid analog/digital precoding for downlink massive MIMO LEO satellite communications," *IEEE Transactions on Wireless Communications*, vol. 21, no. 8, pp. 5962–5976, 2022.
- [10] M. Alsenwi, E. Lagunas, and S. Chatzinotas, "Robust beamforming for massive MIMO LEO satellite communications: A risk-aware learning framework," *IEEE Transactions on Vehicular Technology*, vol. 73, no. 5, pp. 6560–6571, 2024.
- [11] K.-X. Li, X. Gao, and X.-G. Xia, "Ergodic sum rate capacity achieving transmit design for massive MIMO LEO satellite uplink transmission," *IEEE Transactions on Aerospace and Electronic Systems*, vol. 60, no. 3, pp. 3403–3416, 2024.
- [12] A. M. Darya and S. Abdallah, "Semi-blind channel estimation for massive MIMO LEO satellite communications," *IEEE Communications Letters*, vol. 29, no. 1, pp. 75–79, 2025.
- [13] H. Q. Ngo, A. Ashikhmin, H. Yang, E. G. Larsson, and T. L. Marzetta, "Cell-free massive MIMO versus small cells," *IEEE Transactions on Wireless Communications*, vol. 16, no. 3, pp. 1834–1850, 2017.
- [14] Ö. T. Demir, E. Björnson, L. Sanguinetti *et al.*, "Foundations of user-centric cell-free massive MIMO," *Foundations and Trends® in Signal Processing*, vol. 14, no. 3-4, pp. 162–472, 2021.
- [15] H. A. Ammar, R. Adve, S. Shahbazpanahi, G. Boudreau, and K. V. Srinivas, "User-centric cell-free massive MIMO networks: A survey of opportunities, challenges and solutions," *IEEE Communications Surveys & Tutorials*, vol. 24, no. 1, pp. 611–652, 2022.
- [16] M. Mohammadi, T. T. Vu, H. Q. Ngo, and M. Matthaiou, "Network-assisted full-duplex cell-free massive MIMO: Spectral and energy efficiencies," *IEEE Journal on Selected Areas in Communications*, vol. 41, no. 9, pp. 2833–2851, 2023.
- [17] R. Richter, I. Bergel, Y. Noam, and E. Zehavi, "Downlink cooperative MIMO in LEO satellites," *IEEE Access*, vol. 8, pp. 213 866–213 881, 2020.
- [18] K. Humadi, G. K. Kurt, and H. Yanikomeroglu, "Distributed massive MIMO system with dynamic clustering in LEO satellite networks," in *2024 6th International Conference on Communications, Signal Processing, and their Applications (ICCSPA)*, 2024, pp. 1–6.
- [19] V. N. Ha *et al.*, "User-centric beam selection and precoding design for coordinated multiple-satellite systems," in *2024 IEEE 35th International Symposium on Personal, Indoor and Mobile Radio Communications (PIMRC)*, 2024, pp. 1–6.
- [20] Z. Xu, G. Chen, R. Fernandez, Y. Gao, and R. Tafazolli, "Enhancement of direct LEO satellite-to-smartphone communications by distributed beamforming," *IEEE Transactions on Vehicular Technology*, vol. 73, no. 8, pp. 11 543–11 555, 2024.
- [21] Q. Wang, X. Chen, Q. Qi, M. Li, and W. Gerstacker, "Multiple-satellite cooperative information communication and location sensing in LEO satellite constellations," *IEEE Transactions on Wireless Communications*, vol. 24, no. 4, pp. 3346–3361, 2025.
- [22] Y. Zhang and T. Y. Al-Naffouri, "Enabling scalable distributed beamforming via networked LEO satellites toward 6G," *IEEE Transactions on Wireless Communications*, vol. 25, pp. 6666–6680, 2026.
- [23] Q. Shi, M. Razaviyayn, Z.-Q. Luo, and C. He, "An iteratively weighted MMSE approach to distributed sum-utility maximization for a MIMO interfering broadcast channel," *IEEE Transactions on Signal Processing*, vol. 59, no. 9, pp. 4331–4340, 2011.
- [24] Y. Wang *et al.*, "Statistical CSI-based distributed precoding design for OFDM-cooperative multi-satellite systems," *arXiv preprint arXiv:2505.08038*, 2025.
- [25] Q. Zhang, S. Jin, K.-K. Wong, H. Zhu, and M. Matthaiou, "Power scaling of uplink massive MIMO systems with arbitrary-rank channel means," *IEEE Journal of Selected Topics in Signal Processing*, vol. 8, no. 5, pp. 966–981, 2014.
- [26] W. Zhou, D. Zhang, M. Debbah, and I. Lee, "Robust precoding designs for multiuser MIMO systems with limited feedback," *IEEE Transactions on Wireless Communications*, vol. 23, no. 8, pp. 9583–9595, 2024.
- [27] P. Tseng, "Convergence of a block coordinate descent method for nondifferentiable minimization," *Journal of Optimization Theory and Applications*, vol. 109, no. 3, pp. 475–494, 2001.
- [28] M. Grötschel, L. Lovász, and A. Schrijver, *Geometric algorithms and combinatorial optimization*. Springer Science & Business Media, 2012, vol. 2.
- [29] H. W. Kuhn, "The Hungarian method for the assignment problem," *Naval research logistics quarterly*, vol. 2, no. 1-2, pp. 83–97, 1955.
- [30] Federal Communications Commission, "Order and Authorization and Order on Reconsideration: In the Matter of Space Exploration Holdings, LLC, Request for Modification of the Authorization for the SpaceX NGSO Satellite System," Federal Communications Commission, Tech. Rep. FCC 21-48, Apr. 2021, IBFS File No. SAT-MOD-20200417-00037; Call Signs S2983 and S3018; Adopted Apr. 23, 2021; Released Apr. 27, 2021.
- [31] E. Kim, I. P. Roberts, and J. G. Andrews, "Feasibility analysis of in-band coexistence in dense LEO satellite communication systems," *IEEE Transactions on Wireless Communications*, vol. 24, no. 2, pp. 1663–1677, 2025.
- [32] 3GPP, "Solutions for NR to support non-terrestrial networks (NTN) (Release 16)," 3rd Generation Partnership Project (3GPP), Technical Report TR 38.821, December 2019.
- [33] Z. Zhang *et al.*, "Coordinated multi-satellite transmission for OTFS-based 6G LEO satellite communication systems," *IEEE Journal on Selected Areas in Communications*, vol. 43, no. 1, pp. 156–170, 2025.